Provision of Flexible Load Control by Multi-Flywheel-Energy-Storage System in Electrical Vehicle Charging Stations

Sun, Bo; Dragicevic, Tomislav; Andrade, Fabio ; Vasquez, Juan Carlos; Guerrero, Josep M.

Provision of Flexible Load Control by Multi-Flywheel-Energy-Storage System in Electrical Vehicle Charging Stations

Bo Sun, Tomislav Dragicevic, Fabio Andrade, Juan C. Vasquez, Josep M. Guerrero
Microgrids Research Programme www.microgrids.et.aau.dk
Department of Energy Technology, Aalborg University, 9220 – Aalborg East, Denmark
{sbo, tdr, far, juq, joz}@et.aau.dk

Abstract—**Electrical vehicle (EV) chargers are going to occupy a considerable portion of total energy consumption in the future smart grid. Fast charging stations (FCS), as the most demanding representatives of charging infrastructure, will be requested to provide some ancillary services to the power system in order to support basic electrical operation. This paper proposes a local implementation of a hysteresis-based aggregation algorithm for coordinated control of multiple stations that can provide functions such as peak shaving, spinning reserves, frequency control, regulation and load following. Local control is achieved by distributed bus signaling control which exploits multiple flywheel energy storage systems to respond to the system-level control signals without compromising EV charging process. Due to switching nature of the system, a common Lyapunov function has been found in order to prove its stability. Finally, corresponding hardware in the loop results based on dSPACE1006 platform have been reported in order to verify the validity of proposed approach.**

Index Terms—**Fast charging station, plug-in electrical vehicles, flywheel energy storage system, distributed bus signaling.**

I. INTRODUCTION

Since the conventional transportation is mainly based on petroleum and natural gas, the situation of the fossil fuels' cumulative depletion needs to be faced in the future [1]-[3]. To interface the problems ahead, a concept of more electrical vehicles (EVs) was put forward to give a solution for the next generation transportation. It is expected to eliminate the threat of energy crisis and pollution issues. It is estimated that by 2020, the Europe EV Market is going to jump 500%, and up to 35% of the total vehicles in the U.S. will be plug-in EVs (PEVs) according to the Electric Power Research Institute (EPRI) [1]. Since the PEVs are going to play a critical role in future transportation market, it is necessary to provide a suitable environment to accept the huge fleets of PEVs in future smart grids.

Up to now, industry has defined three levels of charging according to different power transfer rates from grid to EV. Among them, fast DC charging stations located on public sites has the most influence on the power system because its power rate is the highest (more than 50 kW [3]). With proper smart charging strategy implemented, the charging stations (CS) are able to eliminate some possible adverse effects on the grid. In addition, multiple CS can be aggregated and utilized to coordinate the interaction with power system and provide ancillary services such as peak shaving, spinning reserves frequency control, regulation and load following.

Recently, an extensive study on system level control of ancillary service provided by demand side management has been shifted into focuses [4]-[6]. As considerable energy consumers, PEVs are also anticipated to provide such services from load side, especially in weak grids formed by intermittent renewable energy sources, such as wind turbines and photovoltaic arrays [6]. In [4], a vehicle to grid (V2G) based aggregation of PEVs is proposed to regulate the charging and discharging rate in order to contribute to the regulation of power system. In [5], PEV charging stations are controlled in unidirectional way to simply switch on or off and modify the aggregated charging pattern according to the command from aggregator. In [6], a hysteresis control originally used for thermostatically controlled load is employed for PEV charging to modify the respective state of charge (SoC). The signals from upper-level controller can shift the SoC band up and down. All the controls strategies above are generated from the system-level viewpoint, and they all share the same serious disadvantage that the charging process of battery pack in PEV has to be compromised when supplying ancillary services to grid. Thereby, the lifetime of PEV battery gets affected more or less [7].

On the other hand, in line with previous work done by the authors, to mitigate the adverse effect on the end-user function of PEV, energy storage system (ESS) is installed within the charging station as an energy buffer in [7]. In that work, flywheel ESS is considered since it is the most suitable technology for providing fast power compensation services. Also, it is a mature and economical technology which has high power density and no degrading problems caused by frequent charging and discharging. Regarding the paralleled ESS control, many works have been done on SoC balance [8], [9]. In this paper, the distributed bus signaling (DBS) control is deployed to realize the coordination between each controller, namely the grid and flywheel controllers.

This paper implements the hysteresis conception originally proposed in [6] on the power electronics level in a local charging station with multi flywheels ESS, as shown in Fig. 1.
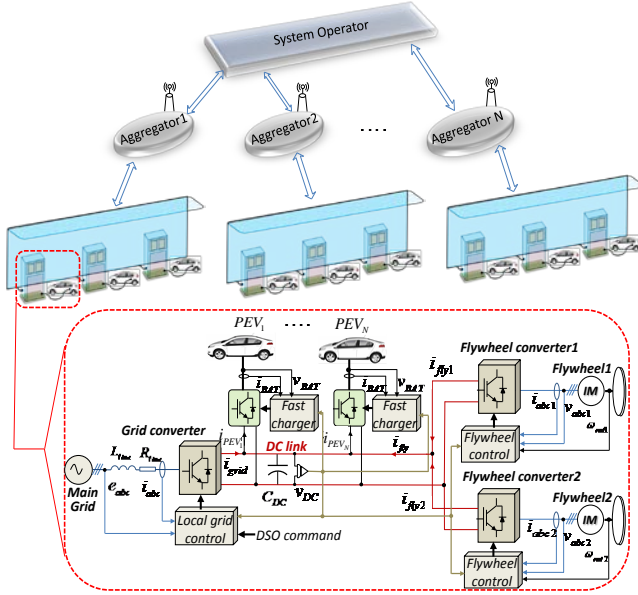
Figure 1. Configuration of the charging station with dedicated flywheel ESS device and system level control scheme

While, the control is realized in a hierarchical structure, this paper's focus is the primary control within the CS respecting the system-level control signals given by the aggregator. Using ESS, the control does not modify the SOC band of battery pack, but controls the energy band extracted from the grid. As a result, the CS upgraded with multi FESS are able to provide the regulation services, while not compromising the regular charging patterns recommended by the battery manufacturers. Consequently, the lifetime of battery is preserved and the PEV user's comfort level remains high. Furthermore, to study the effect of the hysteresis control on the system dynamics stability, a common Lyapunov function based model is assembled. Finally, real-time simulation results verify the feasibility of the proposed strategy for providing ancillary service in CS with multi FESS.

II. CONFIGURATION AND CONTROL OF CHARGING STATION

A. Charging station structure

Fig.1 depicts the basic structure of CS system upgraded with two dedicated FESS, including a set of DC/DC converters serving as PEV chargers and a set of three-phase AC/DC converters connected with grid and paralleled flywheels, respectively. All the power electronics interfaces are connected to a common DC bus. The system dynamics around DC-link capacitor could be derived as follows:

$$C_{DC}\frac{dv_{DC}}{dt} = i_{grid} + i_{fly} - i_{PEV} \tag{1}$$

Where C_{DC} is the capacitance connected to the bus, i_{grid} and i_{fly} are the DC currents flowing from the grid and flywheels, respectively, while i_{PEV} is the current extracted by the fast DC charger(s). The PEV charger, grid converter (GC) and flywheel converter (FC) have their own specific dynamic features, so it is necessary to study the effect produced by each unit, in order to obtain the stability properties of the whole system.

(i) PEV charger. A buck DC/DC converter is applied as PEV charger following the control scheme provided by battery manufacturer which includes constant current and constant voltage charging stages. Since current and voltage only have relationship with battery, this system does not need any feedback signals from FCS. Additionally, a low bandwidth controller is commonly derived since it is not critical to control with a rapid response for PEV charging process. Taking into account all above, the current introduced by the PEV charger may be regarded as a disturbance input that does not affect the system dynamic properties.

(ii) Grid interface. A two-level PWM rectifier is used to connect with the grid, and the control scheme is deployed in d-q reference frame. The DC voltage controller and reactive power controller in this paper generate the I_d and I_q reference. As the stability analysis is derived based on DC-link and only active power exchange is considered in this application, following equation could be obtained:

$$\begin{bmatrix} \dot{i}_d \\ \dot{i}_q \end{bmatrix} = \frac{v_{DC}}{L_{line}}\begin{bmatrix} d_d \\ d_q \end{bmatrix} + \begin{bmatrix} -\dfrac{R_{line}}{L_{line}} & \omega \\ -\omega & -\dfrac{R_{line}}{L_{line}} \end{bmatrix}\begin{bmatrix} i_d \\ i_q \end{bmatrix} - \frac{1}{L_{line}}\begin{bmatrix} e_d \\ e_q \end{bmatrix} \tag{2}$$

where i_q and i_d, d_q and d_d are DC-like currents and duty ratios aligned with q and d rotating axes, respectively, while R_{line} and L_{line} are per phase resistance and inductance of the AC line.

It is assumed that the I_d and I_q reference are followed instantaneously, and considering the grid voltage is synchronized with d-axis and reference for q axis is set to zero, the DC link current from grid could be expressed as:

$$i_{grid} = 1.5\frac{v_d i_d}{v_{DC}} \tag{3}$$

(3) may be linearized around the operating DC voltage, obtaining:

$$\hat{i}_{grid} = 1.5\frac{(e_d + 2I_d R_{line} + I_d L_{line}s)}{V_{DC}}\hat{i}_d \tag{4}$$

I_d is the equilibrium value of i_d

(iii) Flywheel energy storage system. In this paper, two paralleled flywheels based on induction machine are employed, and the parameters and control of two flywheels are the same. The inner control scheme for IM adopts the indirect field oriented control (FOC) which is considered to have a fast and accurate response. The synchronous reference frame is also used for modeling and control of the machine, where d-axis component corresponds to flux and q-axis component corresponds to torque. Based on this classical vector control approach, the d-q model in flux coordinates can be represented as follows:

$$\begin{bmatrix} \dot{i}_d \\ \dot{i}_q \end{bmatrix} = \frac{v_{DC}}{\sigma L_s}\begin{bmatrix} d_d \\ d_q \end{bmatrix} + \begin{bmatrix} -\dfrac{R_s}{\sigma L_s} & \omega_{mR} \\ -\omega_{mR} & -\dfrac{R_s}{\sigma L_s} \end{bmatrix}\begin{bmatrix} i_d \\ i_q \end{bmatrix} - \frac{1}{\sigma L_s}\begin{bmatrix} 0 \\ \omega_{mR}\psi_r\dfrac{L_0}{L_r} \end{bmatrix} \tag{5}$$

where L_s, L_r, R_s, R_r are stator and rotor inductances and resistances, respectively and L_0 is the mutual inductance; i_d and i_q are d and q-axis currents in field coordinates, ω_{mR} is flux rotational speed, i_{mR} is the magnetizing current, while ψ_r is the rotor flux; σ is the total leakage coefficient.
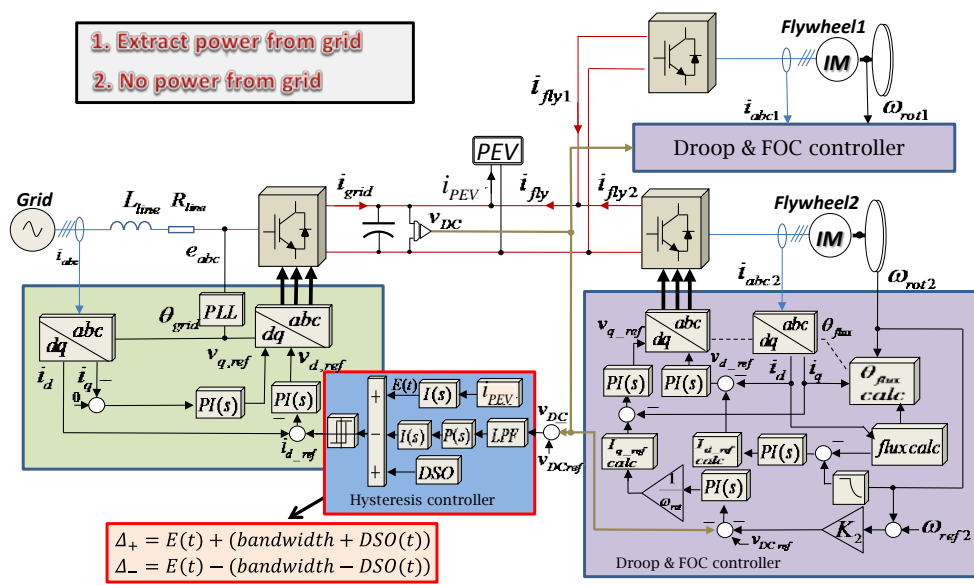
Figure 2. Overall control diagram that incorporates hysteresis controller

The flywheel current flowing towards the common DC bus may be expressed as:

$$i_{grid} = 1.5 \frac{v_d i_d + v_q i_q}{v_{DC}} \qquad (6)$$

The resulting expression around V_{DC} can be linearized as:

$$\hat{i}_{fly} = 1.5 \frac{2\left(R_s + \left(\frac{L_0}{L_r}\right)^2 R_r\right) I_q + \frac{\omega_{rot0} L_0^2 I_d}{L_r} + \sigma L_s I_q s}{V_{DC}} \hat{i}_q \qquad (7)$$

The swing equation of the flywheel governs the changes in the rotational speed of the rotor:

$$J \frac{d\omega_{rot}}{dt} = 1.5 p(1-\sigma) L_s i_{mR} i_q \qquad (8)$$

where J is the flywheel inertia and p is the number of pole pairs.

B. Overall control scheme

In order to provide ancillary services while guaranteeing the regular charging process, the following control objectives are underlined as crucial for deployment of flexible control: 1. Design of decentralized control strategy which makes the flywheels automatically supply the active power 2. Controller can modify the energy extracted from the grid to provide the ancillary services. 3. Plug and play feature for seamless installation of additional PEV chargers and ESS should be inherently incorporated in control and hardware design. The control strategy is implemented in a hierarchical structure, and the complete control block based on distributed bus signaling is deployed within the CS, as shown in Fig. 2.

The speed vs DC voltage droop control is used in flywheel controller. Consequently, the flywheel operates according to the change of DC voltage and flywheels are able to share the active power according to the droop law in a distributed manner. A hysteresis controller similar to [7] is implemented on the grid-side converter, where the algorithm for one PEV charging station can be formulated as follows:

$$\Delta_+ = E(t) + (bandwidth + DSO(t)) \qquad (9)$$
$$\Delta_- = E(t) - (bandwidth - DSO(t)) \qquad (10)$$

with bandwidth being the allowable dead-band around the mean scheduled energy, $DSO(t)$ is the real-time control signal from distributed system operator, $E(t)$ is the total energy requested by the particular charger.

As a result, instead of intermittent charging and discharging in conventional scheme, the system operates in two conditions: extract energy from the grid and no energy output from the grid. In condition 1, the grid supplies the power to the PEV and in condition 2 the multi FESS compensates the power to the PEV according to the DBS control law. Meanwhile, the command signal from DSO is also respected to shift the consumed energy band up and down to request regulation service from the CS. Throughout the whole process, the charging pattern of PEV will not be interrupted.

III. STABILITY ANALYSIS

Caused by the hysteresis control scheme, the system switches between two linear time-invariant subsystems. The small-signal model of two subsystems could be obtained by combining flywheel controller model, grid controller model and upper control loops, resulting in the block diagram shown in Fig. 3. Combining the models of GC and FC presented in (4) and (7) with the loops, belonging to upper control layer (see Fig. 2), the block diagram of control could be obtained in Fig. 3. In the control block, G_1 is obtained from (4) and can be simplified as $G_1 = g_{1p} + s \cdot g_{1d}$, G_2 and G_3 are derived from (7) and can be simplified as $G_2 = g_{2p} + s \cdot g_{2d}$ and $G_3 = g_{3p} + s \cdot g_{3d}$, F is the swing equation in (8). K1 is the proportional gain of GC, K2 and K3 are the droop gains of FC.

Based on the small-signal analysis done by the authors in [7], it is illustrated that the two subsystems are able to work stably with the optimized control parameters. However, the switching may destabilize the whole system even if all individual systems are stable [8]. Hence it is necessary to verify the stability of the switched system. Lyapunov's stability theorem has a direct extension which provides a basic tool for studying uniform stability of the switched system by requiring the existence of a single Lyapunov function whose derivative along solutions of all systems in the family satisfies suitable inequalities.
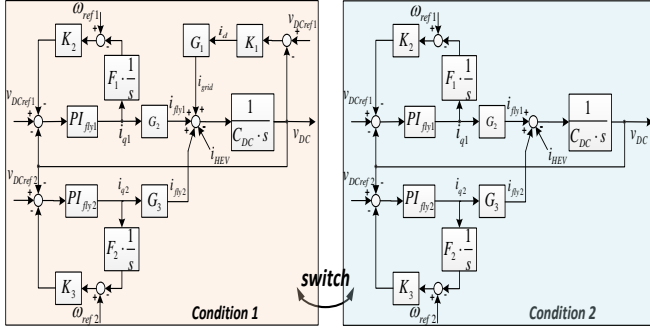
Figure 3. Control model of the system

Suppose that we are given a family f_p, $p \in P$ of functions from R^n to R^n, where P is some index set (typically, P is a subset of a finite-dimensional linear vector space). This gives rise to a family of systems

$$\dot{x} = f_p(x), \qquad \forall p \in P \qquad (11)$$

Given a positive definite continuously differentiable function V: $R_n \to R$, we will say that it is a common Lyapunov function for the family of systems (11) if there exists a positive definite continuous function W: $R_n \to R$ such that we have:

$$\frac{\partial V}{\partial x} f_p(x) \le -W(x) \qquad \forall x, \forall p \in P \qquad (12)$$

Theorem 1 If all systems in the family (11) share a radially unbounded common Lyapunov function, then the switched system has global uniform asymptotic stability (GUAS) [10].

To study the stability of the switched system, the state equations of two subsystems are obtained first.

$$\dot{X} = A_i X + B_i U \qquad i = 1, 2$$
$$X = |x_1 \; x_2 \; x_3 \; x_4 \; x_5|^T \qquad (13)$$
$$U = |V_{ref1} \; \omega_{ref1} \; V_{ref2} \; \omega_{ref2} \; i_{HEV}|^T$$

Where x_1, x_2, x_3, x_4 and x_5 are I_{q1}, ω_1, I_{q2}, ω_2 and V_{dc} respectively.

As the input does not affect the dynamics of system, only A_1 and A_2 need to be considered. Neglecting the lower order of magnitude terms g_{1d} and g_{2d}, A_1 and A_2 can be simplified as follows:

$$A_1 = \begin{vmatrix} 0 & K_2K_{ifly1} & 0 & 0 & -K_{ifly1} \\ F_1 & F_1K_2K_{pfly1} & 0 & 0 & -F_1K_{pfly1} \\ 0 & 0 & 0 & K_3K_{ifly2} & -K_{ifly2} \\ 0 & 0 & F_2 & F_2K_3K_{pfly2} & -F_2K_{pfly2} \\ \frac{g_{2p}}{C_{DC}} & \frac{K_2K_{pfly1}g_{2p}}{C_{DC}} & \frac{g_{3p}}{C_{DC}} & \frac{K_3K_{pfly2}g_{3p}}{C_{DC}} & -\frac{K_{pfly1}g_{2p}+K_{pfly2}g_{3p}+K_1g_{1p}}{C_{DC}} \end{vmatrix} \qquad (14)$$

$$A_2 = \begin{vmatrix} 0 & K_2K_{ifly1} & 0 & 0 & -K_{ifly1} \\ F_1 & F_1K_2K_{pfly1} & 0 & 0 & -F_1K_{pfly1} \\ 0 & 0 & 0 & K_3K_{ifly2} & -K_{ifly2} \\ 0 & 0 & F_2 & F_2K_3K_{pfly2} & -F_2K_{pfly2} \\ \frac{g_{2p}}{C_{DC}} & \frac{K_2K_{pfly1}g_{2p}}{C_{DC}} & \frac{g_{3p}}{C_{DC}} & \frac{K_3K_{pfly2}g_{3p}}{C_{DC}} & -\frac{K_{pfly1}g_{2p}+K_{pfly2}g_{3p}}{C_{DC}} \end{vmatrix} \qquad (15)$$

Now we assume there exists a quadratic common Lyapunov function $V(x)$, then the $V(x)$ must satisfy the following expressions for both A_1 and A_2:

$$V(x) = X^T PX \qquad (16)$$

$$V(x) - \varepsilon(x_1^2 + x_2^2 + x_3^2 + x_4^2 + x_5^2) \ge 0 \qquad (17)$$

$$-\frac{\partial V}{\partial x_1}\dot{x}_1 - \frac{\partial V}{\partial x_2}\dot{x}_2 - \frac{\partial V}{\partial x_3}\dot{x}_3 - \frac{\partial V}{\partial x_4}\dot{x}_4 - \frac{\partial V}{\partial x_5}\dot{x}_5 \ge 0 \qquad (18)$$

Based on the analysis above, MATLAB **SOSTOOLS** toolbox for constructing and solving sum of squares programs (SOSP) with Semi-definite Program (SDP) solver **SeDuMi** [11] is used to search for the common Lyapunov function of the switched system with the parameters in table I. First construct two vector fields $\dot{X}_i$ ($i=1,2$) according to (13)-(15), then define a positive definite polynomial $V(x)$ and SOSP constraints based on (17) and (18), finally the common Lyapunov function solved by **SOSTOOLS** is obtained:

$$V(x) = \begin{vmatrix} x_1 \\ x_2 \\ x_3 \\ x_4 \\ x_5 \end{vmatrix}^T \begin{vmatrix} 0.2932 & 0.06015 & -0.292 & -0.06845 & 0.00018 \\ 0.06015 & 1.897 & -0.06711 & -2.046 & 0.00014 \\ -0.292 & -0.06711 & 0.3 & 0.1725 & 0.00076 \\ -0.06845 & -2.046 & 0.1725 & 4.317 & -0.00275 \\ 0.00018 & 0.00014 & 0.00076 & -0.00275 & 0.0003 \end{vmatrix} \begin{vmatrix} x_1 \\ x_2 \\ x_3 \\ x_4 \\ x_5 \end{vmatrix} \qquad (17)$$

According to the **Theorem 1**, the existence of the common Lyapunov function demonstrates that the whole system is stable with the chosen parameters.

IV. HARDWARE IN THE LOOP RESULTS

A model shown in Fig. 2 has been assembled in MATLAB/SIMULINK and compiled to dSPACE1006 for real time simulation run on sampling time of 10 kHz. All the simulation parameters are listed in the Table I. The results have been extracted in the Microgrid Lab of Aalborg University [12]. In order to demonstrate the performance of the system in reduced time, the simulation is performed in second scale, but in practical application, the time scale should be minutes, as it was shown in [6].

TABLE I. REAL-TIME SIMULATION PARAMETERS

Electrical parameters		Induction machine parameters			
C_{DC}	2.2mF	L_0	10.46 mH	R_s	0.0148 Ω
L_{line}	3.8mH	L_s	10.76 mH	R_r	0.0093 Ω
R_{line}	0.2Ω	L_r	10.76 mH	J	10 kgm^2
$V_{grid}(p-p)$	325V	σ	0.0556		
GC CONTROLLER		**FC CONTROLLER**			
K_1	1.25	ω_{ref}	152 rad/s	T_{fly}	0.0025s
T_{grid}	0.0025s	K_2	0.1	K_3	0.1

The PEV charger was programmed to extract constant current from the DC link which is consistent with the first and the most significant stage in the typical two-stage charging algorithms recommended by battery manufacturers. Due to the hysteresis controller signals, the grid converter output power to DC bus alternates. At the time of 21 sec, signal from DSO changes from 0 to 2 and hence the boundary region is shifted upwards (see Fig. 4). This also causes low frequency oscillation of flywheel speed, as can be seen in Fig. 6 but due to slow outer PI voltage regulator, it again stabilizes around nominal speed.
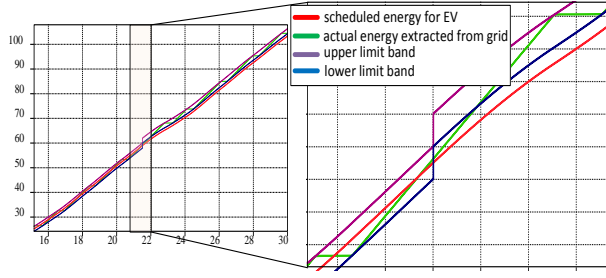
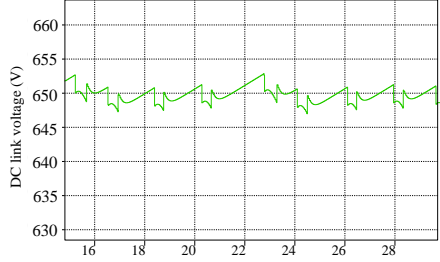Figure 4.   Hystersis control signals
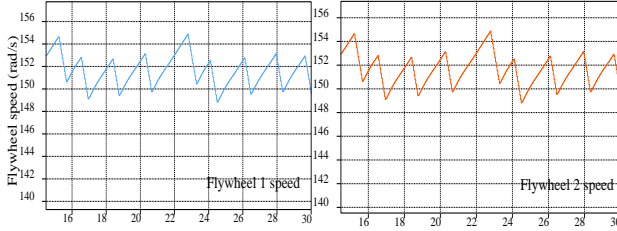

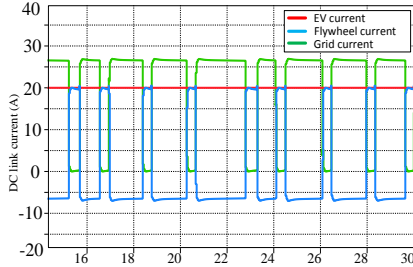Figure 5.   DC link voltage

Figure 6.   Speed of flywheels

Figure 7.   DC link current of PEV, GC and FC

Full propagation of the DC link voltage is depicted in Fig. 5. Maximum deviations from the common value of around 8 V can be observed which is acceptable. However, it should be noted that bigger deviations may appear in practical experimental setup mostly due to delays introduced by the digital control system. Fig. 7 shows that the grid and flywheel alternatively supply the active power to PEV in order to guarantee the PEV charging not affected. Fig 8 shows the grid ac-side current and active power to DC link to demonstrate that the CS's regulation effect on grid.
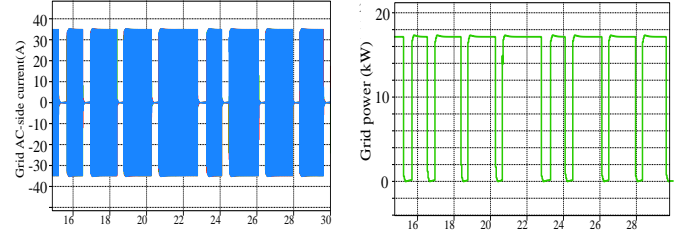

Figure 8.   Grid ac-side current and GC active power

V.   CONCLUSION

This paper presented a flexible load control strategy based on hysteresis controller and DBS in a FCS with multi FESS. As a result, the CS are able to respond to the system-level signals from DSO to provide the regulation services to the power system, while not interrupting the recommended charging algorithm for PEV battery pack. The paralleled flywheels can share the active power requested by PEV according to the droop control during the provision of ancillary service. Furthermore, a Lyapunov based small signal model was assembled to analyze the stability of the system which switches between two linear time-invariant subsystems. Hardware in the loop simulation was performed in order to demonstrate the effectiveness of proposed approach. Research that builds upon the results presented here is currently under way and includes implementation of the algorithm within the practical experimental setup with real converters and flywheel.

REFERENCES

[1]   A. Emadi, M. Ehsani, and J. Miller, Vehicular Electric Power Systems: Land, Sea, Air, and Space Vehicles. The Power engineering, Taylor & Francis, 2010.

[2]   X. Chang, B. Chen, Q. Li, X. Cui, L. Tang, and C. Liu, "Estimating real-time traffic carbon dioxide emissions based on intelligent transportation system technologies," *IEEE Trans. Intelligent Transportation Syst.*, vol. 14, no. 1,   pp. 469–479, 2013.

[3]   M. Yilmaz and P. Krein, "Review of battery charger topologies, charging power levels, and infrastructure for plug-in electric and hybrid vehicles," *IEEE Trans. Power Electron.* , vol. 28, no. 5, pp. 2151–2169, 2013.

[4]   M. D. Galus, S. Koch, and G. Andersson, "Provision of load frequency control by PHEVs, controllable loads, and a cogeneration unit," *IEEE Trans. Industrial Electronics*, vol. 58, no. 10, pp. 4568–4582, Oct. 2011.

[5]   E. Sortomme and K.W. Cheung, "Intelligent dispatch of electric vehicle performing vehicle-to-grid regulation," in *IEEE International Electric Vehicle Conference (IEVC)* 2012, Greenville, SC, USA.

[6]   D. Callaway and I. Hiskens, "Achieving controllability of electric loads," *Proc. IEEE*, vol. 99, no. 1, pp. 184–199, Jan. 2011.

[7]   Tomislav Dragicevic, Stjepan Sucic, Juan C. Vasquez, Josep M. Guerrero, "Flywheel-Based Distributed Bus Signalling Strategy for the Public Fast Charging Station", *IEEE trans. smart grid*, vol.5: no.6. pp.2825-2835, Nov. 2014.

[8]   Xiaonan Lu; Kai Sun; Guerrero, J.M.; Vasquez, J.C.; Lipei Huang, "State-of-Charge Balance Using Adaptive Droop Control for Distributed Energy Storage Systems in DC Microgrid Applications,"*, IEEE Trans. Ind. Electronics*, vol.61,no.6, pp.2804-2815, June 2014

[9]   H. Kakigano, Y. Miura, and T. Ise, "Distribution voltage control for dc microgrids using fuzzy control and gain-scheduling technique,"*, IEEE Trans. Power Electronic*, vol. 28, no. 5, pp. 2246–2258, May 2013.

[10]   D. Liberzon, Switching in Systems and Control. Boston, MA: Birkhauser, 2003.

[11]   S. Prajna and A. Papachristodoulou, "Introducing SOSTOOLS: A general purpose sum of squares programming solver," in *Proc. IEEE Conf. Decision Control*, Las Vegas, NV, 2002, pp. 741–746.

[12]   Aalborg University, Dept Energy Technology, Microgrids research programme www.microgrids.et.aau.dk